Development of an organic photovoltaic energy harvesting system for wireless sensor networks; application to autonomous building information management systems and optimisation of OPV module sizes for future applications

Zhang, Shoushou; Bristow, Noel; David, Tudur Wyn; Elliott, Fergus; O'Mahony, Joe; Kettle, Jeff

Solar Energy Materials and Solar Cells

DOI:
https://doi.org/10.1016/j.solmat.2021.111550

Published: 01/03/2022

Peer reviewed version

Development of an organic photovoltaic energy harvesting system for wireless sensor networks; application to autonomous Building information management systems and optimisation of OPV module sizes for future applications

Shoushou Zhang[1], Noel Bristow[1], Tudur David[1], Fergus Elliott[1], Joe O'Mahony[2], Jeff Kettle[3]

1 School of Computer Science and Electronic Engineering, Bangor University, Dean Street, Bangor, Gwynedd, LL57 1UT, Wales

2 PMBRC, Waterford Institute of Technology, Cork Road, Waterford City, Ireland

3 James Watt School of Engineering, University of Glasgow, Glasgow, Scotland

Abstract

The emergence of internet of things (IoT) has motivated research into developing Organic Photovoltaic (OPV) devices that can efficiently convert indoor light into electricity. In this work, the performance and operation of an OPV-powered Wireless Sensor network (WSN) for Building Information management system is provided through a case study. Results are shown for the operation of the WSN and how data can be acquired to build machine learning algorithms that can forecast the indoor conditions of a building, when the system is linked to an external weather station. Remarkably, our data indicates only minor degradation of the OPV when tested under indoor conditions over a 21-month period; at a luminance level of 1000 Lux, only a -10% relative drop in performance was measured. Finally, the field data is used to optimise the size of the OPV and battery for future indoor applications which possess different energy loads. Based on the energy efficiency model, the loss of power supply probability (LPSP) of the indoor applications system is calculated for different size combinations of PV, battery sizes and load energies. This model provides a method to calculate the required OPV output power to ensure remote operation of other IoT electronics.

Keywords: organic photovoltaics (OPV), energy harvesting, wireless sensor network, internet of things (IoT), forecasting, machine learning,

1. Introduction

With the growing development of the Internet of Things (IoT) applications, organic photovoltaics (OPVs) are seen as a highly desirable technology for powering many indoor applications due to their high efficiency when operating under indoor conditions [1,2, 3]. Indoor light sources possess a much narrower emission spectra and lower intensity of light. This provides an opportunity for OPV modules, whose performances are higher than mature PV technologies for low ambient light or artificial light environments as they can be 'tuned' to operate more efficiently under these conditions. Currently, the record power conversion efficiency (PCE) of an OPV module is 31% under indoor test conditions [4] and OPVs possess excellent indoor stability as they are not exposed to outdoor levels of UV and humidity, which have been shown to adversely impact their stability [5]. The timing of these record indoor efficiencies is apt; over the past few years, an exponential growth of Internet of Things (IoT) components and connectivity solutions has been proposed. These could enable a broad array of sensors to monitor, report back readings, or actuate remote electronic

systems. In order for such sensor networks to be easily deployed and to be autonomous for long periods they need to be both wireless and capable of energy harvesting, otherwise the costs of deployment and maintenance would far outweigh any benefits [6]. IoT networks can be built using various communication technologies, depending on the specific requirements (data rate, range, security etc).

Whilst a number of studies have been conducted into OPV indoor performance and the physical reasons for greater efficiencies in indoor conditions, there are few reports of actual deployments and example applications. One potential application is for use in smart or low carbon buildings. The International Energy Agency stated in a recent report that indirect and direct emissions from buildings continue to rise, reaching 10GtCO_2 in 2019, accounting for 28% of total global energy-related CO_2 emissions [7]. The demand for energy in buildings from heating, ventilation and air conditioning (HVAC), as well as lighting and other systems, can be reduced by digitalisation. This involves using large arrays of sensors to gather data which can be processed by artificial intelligence to improve the efficiency of the control systems managing the building [8]. Smart buildings controlled by intelligent Building Information Management Systems (BIMS) can use meteorological forecasts and artificial neural networks to predict energy demands, and this can be used to reduce energy consumption and improve sustainability as well as enhancing user comfort [9]. Whilst new buildings can be designed to accommodate new sensors, by potentially even embedding them into the building material, older building stock requires innovative solutions to gather the data and inform building managers. Such BIM sensor systems offer an ideal application for OPV energy harvesting; the data rate is low-medium (depending on the sensor and configuration), and the data transmission range is also low. Therefore, low power modules are suitable and the sensor systems can use ambient indoor light to harvest energy [10].

This paper investigates the design of Wireless Sensor Nodes (WSN) for measuring indoor environmental conditions through a case study of a 1960s building. The WSN was entirely powered by OPV modules over an evaluation period of 18 months from June 2019 to January 2021. The results from the deployment of these modules, along with outdoor weather station data, were used to train machine learning algorithms, which allows the BIMS to predict energy patterns within the building and acquire data so that building users/managers can optimise the energy usage. Finally, the effectiveness of the organic solar module for powering the WSNs is examined and the indoor data acquired is used to optimise the sizing of the OPV module and back-up battery.

2. Experimental setup

2.1 Wireless Sensor Design

The data for this project was obtained using environmental WSNs designed in-house. The sensors comprise three main elements: a set of real-time sensors for measuring the local environment, a wireless communication module for sending the data to a central datalogger, and energy harvesting to maximise energy efficiency. The sensor was designed around the ATmega238P microcontroller (MCU), as this allowed rapid prototyping. The following environmental sensors were included, with election based on their low power requirements and accuracy: TSL2591 to measure light levels (in lux), BME280 to measure temperature, humidity and air pressure, and a COZIR-A to measure CO_2 levels (ppm). The node also has a DS3231 real-time clock (RTC) to ensure accurate sleep intervals and an ADS1015 to monitor battery voltage. The lithium polymer (LiPo) battery (supplied by Conrad Energy) is kept charged using a flexible OPV module (supplied by InfinityPV, Denmark) along with an

SPV1050 charge controller, and the performance of the solar module is monitored using an INA226 current, voltage and power sensor. The node uses a ZigBee RF module to transmit the sensor measurements back to a central datalogger via a star network configuration. ZigBee has the advantages of easy deployment, ability to form flexible mesh networks and a high data rate. The relatively low transmission range (50-200m) was not a problem in the environment being monitored, and all the sensor nodes were able to communicate back to a coordinating ZigBee module, connected to the datalogging PC. Figure 1a shows a WSN powered by a flexible OPV module.

An important aspect of the design was to minimise the power consumption, so that the node could be powered by an OPV module under indoor lighting levels, maintaining the battery charge level and ensuring long-term and autonomous operation. Although the node can consume over 100mW when it is actively transmitting data it requires only 0.7mW when it is in sleep mode. This was achieved by using sensors capable of low power sleep modes, an IC load switch to turn off the CO_2 sensor, and putting both the ZigBee and MCU into sleep mode in between measurements. The only component which stayed awake was the RTC, which toggled a hardware interrupt on the MCU after a set period had elapsed, allowing the next measurement cycle to be initiated. The CO_2 sensor required careful management, as it required several seconds to warm up and it then needed to take a number of measurements at 0.5s intervals in order to report a filtered or averaged measurement. Filtering was required to improve the accuracy of the transmitted measurement, as the CO_2 sensor measurements are quite noisy (within the confines of the device's ±50 ppm resolution). In order to further reduce power consumption the node employs other active power management strategies: i) increasing the interval between transmissions to 5 minutes when the environmental conditions are deemed stable and have not changed significantly since the last measurement (±5%); ii) increasing both the sampling and transmission interval to 15 minutes when the light levels are very low and the room is unlikely to be occupied; iii) increasing the sampling/transmission interval to 30 minutes when the battery is determined to be low in charge (below 20% capacity). Whilst it was not implemented in these trials, power consumption could be further removed by only switching on the CO_2 sensor when data was going to be transmitted, based on the assumption that if the other environmental conditions had remained stable it was unlikely that CO_2 had changed significantly. A schematic diagram showing the interconnection of the components is shown in 1b.

2.2 Testing and setup

Two nodes were installed in the School of Computer Science and Electronic Engineering, communicating with a ZigBee module setup as a coordinator and connected to a datalogging standalone PC. In order to build the forecasting algorithms, outside conditions were monitored using a Davis Vantage Pro 2 weather station, which was used to collect meteorological data including temperature, humidity, wind speed and direction, solar irradiation, UV, rainfall, and air pressure. The weather station data, sampled once per minute, and the intermittent data from the wireless nodes are both loaded onto an MS Access database, where they were synchronised, so that datasets could be obtained comprising the nearest weather station record, while the monitoring data obtained from each wireless node. These datasets were then extracted and analysed using machine learning (ML) in Python as described below.

The synchronised datasets were extracted from the MS Access database and consisted of the following fields:

- Data from the wireless sensor nodes (these were the fields to be predicted)
    - temperature, humidity, light levels, CO_2 concentration
- Data to be used as the basis for the predictions:
    - Outdoor weather data: temperature, humidity, dew point, wind speed, wind direction, barometer, rainfall, irradiance, UV index & dose.
    - Extra attribute: building heating (On/Off codified as binary).

2.3 Machine learning approaches

ML regression algorithms were used to perform the forecasting analysis; whilst several algorithms were trialled, especially Extra Trees Regression, the work focused on Random Forest. The Python language (version 3.7) was used to perform the ML analysis, as it has many suitable library modules for both numerical analysis and plotting: Pandas, Numpy, Matplotlib, Scipy, Scikit-learn and Datetime. The ML algorithms were implemented using the Scikit-learn Python package. The Random Forest (RF) algorithm was employed as a suitable ML algorithm for time series forecasting [11]. The RF algorithm can be considered as an ensemble of individual decision trees [9]. A decision tree operates by applying a cascade of criteria to each feature of the dataset and identifying which of these criteria are fulfilled. The decision tree is comprised of several components, namely decision and prediction nodes. Dependent on the criteria which have been identified for each feature, the decision tree applies a class label, based on the fulfilled criteria. In the case of performance prediction and forecasting, a continuous variable decision tree is employed where the decision tree has a continuous target variable and the performance parameter output is predicted based on continuous variable inputs [12]. Finally, the RF collects all the outputs from each individual tree and reaches a collective prediction based on the majority vote from each decision tree. In the case of continuous variables, the output value is determined through averaging of the outputs from each tree.

The RF algorithm allows for averaging of multiple deep decision trees such that overfitting of the data is avoided; deep decision trees tend to become highly attuned to irregular patterns in datasets and, consequently, have very low bias, but high variance. The averaging process in the RF algorithm is referred to as feature bootstrap aggregation bagging [13]. Initially the dataset is split into a training set and a testing set, where the RF algorithm is first trained and a predictive model developed. Subsequently, the model is applied to unseen data in order to predict and forecast the indoor conditions. Feature bagging is a modified version of the bagging process used for decision trees, where for each split in the decision tree learning process, a random subspace of the features is selected [14]. This reduces the likelihood of a limited number of strong predictors becoming selected by the majority of the decision trees, leading to correlation of these features. The process of feature bagging is summarised below.

Considering a training set consisting of $X = x_1, x_2, \dots, x_n$ attributes and $Y = y_1, y_2, \dots, y_n$ responses, bagging selects L random samples of X and applies a decision tree to each sample. For $l = 1, \dots, L$, n training samples are randomly selected with replacement, meaning that a feature may be repeated more than once in a particular sample. A regression decision tree (f_l) is subsequently trained on the random samples. Once the model has been trained, it can be applied to the unseen testing data with samples x'

$$\hat{f} = \frac{1}{L}\sum_{l=1}^{L} f_l(x'), \quad (1)$$

where $\hat{f}$ is the averaged prediction from all the sampled decision trees. This methodology of bagging RF algorithms allows for predictions to be made with low variance whilst minimising the bias.

2.4 Solar energy harvesting using Organic Photovoltaics (OPVs)

An OPV modules was used for this work and was based on the "infinityPV foil" made by InfinityPV ApS of Jyllinge, Denmark. These flexible solar modules are produced in various lengths according to the desired output power. The particular module used was based on the 110mm wide bisectional films which was cut to a length of 230mm. The output performance, stability and energy yield is discussed in section 3.

3. Results

3.1 Monitoring performance

Data analysis was conducted over two periods: summer 2019 and winter 2019/20, although the WSN was operational for 18 months. The nodes were located in two rooms at the School of Computer Science and Electronic Engineering at Bangor University; a north-east facing laboratory and a south-west facing office. The building is typical of 1960's concrete office blocks, with full-width single-glazed windows, poor insulation and draughty (see Figure 3). Such a building is ideal for BIM system deployment as the energy efficiency would be low, so minor adjustments in the building operation could yield substantive reductions in the energy footprint.

Figure 2 shows temperature and relative humidity results from both rooms, as well as relevant outdoor measurements obtained from the OPV-powered WSNs. Data was transmitted to a computer in the office of the authors so real-time monitoring was possible. It can be seen that the office is affected by its SW aspect and has high diurnal swings in temperature, compared to the laboratory which is less influenced by outdoor conditions (temperature and irradiance). The winter data shows how the building is affected by poor insulation, with the indoor temperatures dropping by several degrees when the building's heating system is turned off; this occurs at weekends and over extended holidays when the department is shut (it was noticed that the heating came on for two days over the Christmas break, presumably in response to the low outdoor temperatures). The relative humidity (RH) follows similar patterns, with the office having the larger diurnal swings; RH has an inverse relationship to temperature. Indoor RH is not unduly affected by rainfall.

Figure 3 shows indoor light levels (measured in lux) and outdoor irradiance. The graphs are plotted for just a few days, as otherwise the data overlaps and some of it becomes obscured. It can be seen that the NE facing lab has lower indoor light levels overall, which peak in the morning (when the sun is in the East) and the SW-facing office has higher overall light levels which peak in the afternoon. The winter data shows that when the rooms are occupied the light levels are maintained at a minimum of about 400 lux using artificial lighting. This is the low level of energy that solar cells used for indoor harvesting can expect in winter. It can also be seen that the peak light levels in the office are similar in both winter and summer; although the irradiance levels are much lower in winter (the outdoor irradiance is measured using a horizontal sensor which will exacerbate this effect) the office benefits from the sun being lower in the sky.

These results all show that the SW facing office is more affected by outdoor conditions, both because it faces the sun for most of the afternoon and because it faces the prevailing wind direction; these lead to large diurnal swings in temperature, and this in turn leads to reverse swings in RH. The laboratory, by contrast, faces NE, away from the sun and prevailing wind. The lab has a smaller floor area than the office (by a factor of about three) and therefore the ratio of external glazing to internal walls is lower. These factors all lead to the laboratory having a much more stable internal climate, less affected by outdoor conditions.

3.2 Forecasting of internal conditions based upon climatic and OPV-powered WSN data

Data from the WSN was sent to a data logging PC and was synchronised with outdoor meteorological data. Using this combined data set it was found that just two weeks of data was needed to enable ML-algorithms to be generated that accurately predicted the future indoor environmental conditions based upon meteorological weather conditions. This was the same for each parameter. For training purposes, the ML algorithms were trained using outdoor climatic conditions as well as information regarding whether the heating is on or off in the building (codified in binary) in order to predict each of the different indoor conditions (temperature, relative humidity, CO_2 concentration and illuminance). The learnt models were then applied to future days of data, constituting the testing set, in order to forecast each of the indoor conditions.

The indoor and outdoor data were processed using the Random Forest (RF) machine learning algorithms to examine whether the indoor conditions could be predicted based on outdoor climate. Forecasting was processed for temperature, humidity, light levels (illuminance) and CO_2 concentration. Figure 4 shows the RF forecasting results for temperature in the office during the summer. The Pearson coefficient of correlation (CC) and root mean square error (RMSE) have been calculated for all datasets; CC measures the linear correlation between the two datasets. A value of CC close to 1 indicates that the model is a very good fit to the actual data and above 0.5 is a reasonable fit. Figure 4(b) shows the actual vs. predicted temperature for the training set and shows a good linear correlation (CC_{RF}=0.999), which indicates that the model is consistent with the training data. Figure 4(c) shows the actual vs. predicted temperature for the testing set and both show a reasonable correlation (CC_{RF}=0.813), indicating that the model is usable for forecasting indoor temperatures.

In Table 1 CC for RF data are shown for both training and testing sets for all parameters, locations, and seasons (based on 2 weeks of training data and 2 weeks of testing data). All of the CC values for the training sets were close to 1, indicating that the models were well trained. The testing results for each parameter can be examined individually by considering the CC fits. It can be seen that temperature and irradiance predictions showed the best fits with CC of 0.65-0.9, regardless of season or location. For temperature, summer generally gives a better fit than winter whilst for illuminance, the office gives a good fit in both seasons and there is little difference between the office and the lab. The illuminance in the lab is predominantly governed by the interior lights, as discussed later. For humidity, only the summer data appears to give a good fit, whereas for the CO_2 concentration only the office during winter gives a reasonable fit; during summer the CO_2 prediction and has a low CC and is difficult to predict. This is not surprising as this is largely governed by room occupancy so additional PIR sensors are really needed to accurately forecast CO_2 levels, as the lab was frequently unoccupied.

The data in table 1 show that the environmental factors in the office can be forecast, whereas those for the lab are slightly less predictable. Figure 5(a) shows an aerial view of the School of Electronic Engineering, showing the position and aspect of both the office and lab (image taken from [15], details of location are found in [16,17]). Figure 5(b) shows a detailed floorplan of both rooms. Taking into account that the exteriors of both rooms consist of full width windows (from mid-height to ceiling) it is clear that the office has a much higher proportion of exterior wall/window surface area. If we also take into account the aspect of each room and the fact that the windows are single-glazed, it can be understood why the environment of the office can be predicted from outside conditions, whereas the environmental conditions in the lab are not as readily predicted by outdoor conditions.

Parameter	**Location**	**Season**	**CC_{TRAIN}**	**CC_{TEST}**
Temperature	Office	Winter	0.999	0.813
		Summer	0.999	0.86
	Lab	Winter	0.998	0.695
		Summer	0.998	0.820
Illuminance	Office	Winter	0.997	0.758
		Summer	0.999	0.891
	Lab	Winter	0.988	0.705
		Summer	0.992	0.720
Humidity	Office	Winter	0.999	0.691
		Summer	0.999	0.775
	Lab	Winter	0.996	0.604
		Summer	0.997	0.740
CO_2	Office	Winter	0.962	0.524
		Summer	0.977	0.407
	Lab	Winter	0.990	0.601
		Summer	0.998	0.360

Table 1: Correlation Coefficient (CC) values for Random Forest (RF) results are shown for the both training and testing sets for all parameters, locations, and seasons (based on 2 weeks of training data and 2 weeks of testing data). The data shows how the OPV-powered BIM WSN can be used to forecast indoor conditions based upon outdoor meteorological data

3.3 Solar Energy harvesting

The performance of the OPV module under indoor conditions is shown in Figure 6, which details the maximum power point as a function of indoor irradiance of the OPV, based upon measurements conducted in the room which was used for the experiments. The room is equipped with Phillips 4000k (cool white) LED lights [18]. All OPV performance measurements were calibrated using a PCE-Instruments Americas Luxmeter, to ascertain the luminance in the room. It is worth pointing out that

there is likely to be some seasonal and diurnal variation in the light spectrum within the room but this data provides a good guidance for the performance of the modules used in this work.

In Figure 6, the performance of the OPV modules at 21 months after the start of the test is also shown. It is interesting that there is almost only minor degradation observed over this time period. At higher luminance values, a small drop was noted; for example, at 1000 Lux, a 10% relative drop in performance was observed. Based upon previous studies, OPV degradation is largely governed by humidity, light (especially UV radiation) [19] and condensation [20], but these are all severely reduced in an indoor setting and the ambient temperature rarely exceeded 30°C. The indoor environment is much more benign than the outdoors according to many of the accelerated ISOS consensus standards tests, which accounts for the high stability. The results show the OPV modules are highly stable under indoor conditions. Indoor environment appears slightly greater at lower luminance values; for example at 200 Lux, a 24% relative drop in performance was measured. Nevertheless, from our experiments more than70% of the power generation occurs when the irradiance levels greater than 800 Lux, so this is not a minor deterioration at lower irradiance levels, and itis not a concern for long term deployments.

Data was collected over the test period to assess the effectiveness of the OPV for powering the WSN. The module was deliberately oversized so that the WSN would always be powered and no data would be lost. However, the methodology used allows us to estimate the module size and power requirements for future system design; as discussed the performance of the solar module was monitored using an INA226 power monitor connected to the microcontroller. The instantaneous OPV power was reported each time a measurement was made, based on the sampling rate at that time.

Figure 7(a) shows the diurnal energy yield and the battery voltage over a three-month period in winter. It can be seen that the battery doesn't drop substantially in capacity throughout this period. The battery is lithium polymer (LiPo) with a nominal voltage of 3.7 V and a capacity of 1000mAh. Additionally, no drop in daily yield is observed over the course of the test, illustrating that the modules were stable over the operational time. However, the low light performance does display a slight decrease. Shown in Fig 7(b) is the power consumption of the WSN during a sensing cycle; a number of peaks are present from $t = 5\ secs$ until $t = 10\ secs$ due to the operation of the CO_2 sensors, which is based on a Non-Dispersive Infrared Sensor. The sensor has a warmup instability which takes 10 seconds to approach a final steady state output. This instability is most likely due to pressure changes from the measurement, as the infrared light source heats the gas and causes a slight pressure variation thus modifying the diffusion. From $t = 10\ secs$ until $t = 12\ secs$, there is a relatively prolonged period of power consumption as the WSN transmits data via the ZigBee. In between measurements, the WSN is sent to sleep with minimal power consumption $(P_d = 0.7mW)$. Figure 7(c) shows the number of transmissions per day over a four-week period and highlights the effect of a firmware update in improving the adaptive sensing rate leading to a sharp drop in the number of transmissions, from an average of about 350/day to between 60 and 70 transmissions per day. Finally, figure 7(d) shows the effect that this has on the diurnal energy requirements of the node. Although there is a drop in the energy requirement when the transmission rate reduced (from about 25mWh/day to about 18mWh/day), it is clear that the main factor is the energy demand when the unit is in sleep mode (~16mWh/day) (Figure 7b). By

comparison the energy used for each transmission is only 0.028mWh, which adds about 2mWh/day once the firmware updates were implemented.

3.4 Optimisation of OPV sizing

3.4.1 Methodology

In this work, a comparison of the average daily energy requirements during winter months of the node (18mWh) and the average daily PV yield (57mWh) show that the deployed OPV module was capable of keeping the WSN fully operational even when light conditions were curtailed. The OPV was deliberately oversized in order to ensure the energy demands of the WSN was always met by the OPV in these months. However, using the acquired data of the battery state and OPV yield, the optimal size of an OPV module and battery can be estimated for any stand-alone system, even when different load requirements or OPV power output (due to different power conversion efficiencies or siting of the solar panel) are present. Our aim is to use the data to provide an approximate guide to researchers who are seeking to use indoor PV modules for a variety of applications.

There have been a number of efforts to calculate the optimal size of PVs for outdoor applications [21], but very few for indoor examples. To achieve our goal, we have adopted the methods of *Shen* who developed a procedure to calculate the optimal sizes of stand-alone PV/battery systems using the measured field data [22]. To quantify the performance of new PV/battery combinations, the 'loss of power supply probability' (LPSP) parameter is used, which indicates the probability that the load demand of our standalone system cannot be satisfied by the OPV/storage system.

Table 2 provides a summary of the conditions used for acquiring the data in this work. The average luminance in the room during the measurement campaign was 144 Lux (including night-time hours), and 266 Lux during office hours (from 8:30am to 17:00pm). Our WSN operated 24 hours per day, however if it was designed so that it switched to a sleep mode outside of office hours, such that the PV module size could be reduced further. In this work, the battery charge efficiency is supposed to be the round-trip efficiency, and the battery discharge efficiency is supposed to be 100%.

For the optimisation, we assume that the WSN will outlive the OPV and battery (typically one can expect 10 years lifetime from such a system installed indoors). However, our sizing assumes that the OPV degrades at -5% per annum and the battery degrades at -10%. In the case of the OPV, this is set based on the experimental data from section 3.3. In the case of the battery, we have used the manufacturers data. Whilst we assume this is 'best case' degradation rate, it is worth noting that we have set the depth of discharge (DOD) on the system to 50% as this is known to prolong the life of the battery. It is worth noting that if the battery has been depleted and the WSN was being started from this state, a short period exists (1-2 mins) where there is slightly greater power draw from the system (around 25% of the normal value). This doesn't effect the overall model conclusion as we assume the battery always has some charge.

Finally, whilst the data shown in figure 7 refers to winter month performance, the battery sizing has been conducted based on a full year of field data. In the UK, the winter corresponds to the

season when the OPV is generating the least amount of power, nevertheless the data refers to the probability of power loss over the course of a full year.

Key parameter for initial model data	**Value**
Average daytime luminance (8:30 to 17:00)	266 lux
Average 24 hour luminance	144 lux
Maximum power point at 200 Lux	0.32 μW/cm^2
Maximum power point at 1000 Lux	4.51 μW/cm^2
Assumed OPV and battery deterioration	-5% relative reduction per annum
OPV module size	253cm^2
Battery size	1000mAh
Assumed battery discharge efficiency	100%
Average daily load consumption	18mWh

Table 2: Measured parameters used that field data was acquired with and used in the OPV/battery size optimisation model

Using the data acquired from the WSN including the hourly OPV energy yield, battery state and power consumption of the WSN, the size of the OPV module and battery can be optimized in order to ensure that there is enough energy to maintain the WSN in an on-state (i.e. LPSP > 0.01). There are two events that required adjustments in the battery state for our system; firstly, *charging*; if the energy generated by the OPV is greater than that of the load requirement, then the excess energy is stored in the battery (unless the battery is already at full charge). During the *charging* cycle, the value of the energy reserved in the battery at a particular hourly interval, *n*, will be;

$$E_{B(n)} = E_{B(n-1)} + \left(E_{PV(n)} - E_{L(n)}\right) \times \eta_{batt} \qquad (1)$$

When the energy generated by the OPV is smaller than the load requirement, the battery *discharges* as it powers the WSN. During this discharging cycle, the value of the energy reserved in the battery at a particular hourly interval, *n*, will be;

$$E_{B(n)} = E_{B(n-1)} - \left(E_{L(n)} - E_{PV(n)}\right) \qquad (2)$$

where:

$E_{B(n)}$ - the energy reserved in the battery during an hour interval, n ,

$E_{B(n-1)}$ - the energy reserved during the previous hour interval $n-1$,

$E_{PV(n)}$ - the energy generated by OPV module during an hour interval n ,

$E_{L(n)}$ - the energy demand of load during an hour interval n ,

η_{batt} - the charge efficiency of the battery,

The constraints of the energy reserved in the battery during an hour interval, *n*, would be:

$$E_{B\min} \le E_{B(n)} \le E_{B\max} \qquad (3)$$

According to the state of charge of the battery, the mathematical equation of the loss of power supply probability (LPSP) can be expressed as

$$LPSP = P\left\{E_{B(n)} \le E_{B\min}, n \le N\right\} \qquad (4)$$

where $E_{B\min}$ is the minimum allowable energy level in the battery. The LPSP is the probability that the state of charge at any hour during the day within a cycle of *m* days (N hours in total), is less than the minimum allowable energy $E_{B\min}$ which would cause the WSN to switch off. The LPSP can be expressed as

$$LPSP = \frac{\sum_{n=1}^{N} LPS_{(n)}}{\sum_{n=1}^{N} E_{L(n)}} \qquad (5)$$

where $LPS_{(n)}$ is the loss of energy supply during an hourly interval, n , which can be represented as

$$LPS_{(n)} = E_{L(n)} - (E_{PV(n)} + E_{B(n-1)} - E_{B\min}) \qquad (6)$$

3.4.2 Results of the OPV sizing

The LPSP of the stand-alone solar system has been calculated using equation (5) to assess the different combinations of OPV, battery and load sizes in order to ensure the desired LPSP is obtained. A flowchart for the process used to calculate the LPSP is shown in Figure 8 [20]. By adjusting the OPV size, battery size or load demand, the LPSP of the system can be estimated.

Figure 9(a) shows how the OPV module size and load demand (at a fixed battery size 3700mWh) impact on the LPSP values. The expected trend exists; as the load demand increases, the required OPV size to meet that energy demand has to increase, otherwise the probability of power outages increases. In order to ensure that the WSN always remains on, the LPSP must remain at 0.01; this condition is highlighted by the red line and any combination of OPV size and load demand below the yellow line will ensure that an LPSP value of 0.01 is maintained. As a reference, the OPV size and required load energy needed for this application is marked on the graph. It is clear that with the selected OPV size and energy demand of the BIM WSN, the system would always be on.

Ensuring that the LPSP remains at 0 is vitally important to ensure that the OPV/battery system can supply the energy demanded by the load. As a result, figure 9(b) shows the minimum load demand that can be met by a particular combination of OPV size and battery size in order to ensure that an LPSP of 0.01 is obtained. For example, if a particular load demand was known, the minimum OPV size and battery size (in order to ensure LPSP is 0.01) could be selected based on this data. In practice, designers of standalone systems would want to add a safety margin into design configurations, so a moderately oversized battery and/or OPV is needed to account for any variations in performance or degradation in performance. As an example, the red line indicates the range of OPV sizes and battery sizes that could have met the load requirements of the BIM WSN used in this work. The red cross (marked on Fig. 9(b)) indicates the OPV and battery size used in this work, which could have ensured an LPSP < 0.01 is maintained for a system with a demand up to 143mWh.

Conclusions

This paper reports the first demonstration and performance monitoring of an indoor application of an OPV module. A case study is presented, where wireless sensor nodes have been powered by OPV modules for 18 months to monitor the indoor conditions of an office building and incorporated into a building information management (BIM) system. The nodes were successfully deployed over 18 months (covering both winter and summer) in two different rooms in a 1960's concrete office building, communicating via ZigBee to a central datalogging system. Power consumption was optimised by the use of various strategies including adaptive sensing and sleep management. Using the central logger, the indoor results were analysed using a Random Forest machine learning algorithm which enabled prediction of the indoor conditions when the data logger was synchronised with an outdoor meteorological measurement setup. Investigation of the charging performance of the OPV module was used to optimise the sizing of OPV modules and battery systems needed for stand-alone energy harvesting systems. Such data could provide vital guidance for designers of indoor systems in the future. The OPV module showed remarkable stability over the measurement campaign, proving clear evidence that indoor applications of OPV could be an excellent market opportunity for this solar technology.

We see this work as a promising first case study of using OPVs for an indoor application where the operation is monitored over an extended period of time. In terms of cost competitiveness, OPV is not currently competitive ($1.6/$W_p$ [23] for OPV compared with <$0.25/$W_p$ for Silicon [24]). However, there is great potential as the technology evolves with projected costs of $0.23/$W_p$ [25] but which could potentially drop further with greater usage in applications such as these. In addition, silicon modules are designed for outdoor power generation and the cost is higher for similar sized indoor energy harvesting modules (which are typically >$1/Wp from electronic suppliers). In addition, the OPVs outperform crystalline silicon cells indoors since the ultra-thin nature of OPV solar cells lead to a strong absorption against UV-visible spectrum and has strong spectral matching with indoor lightings [26].

An additional matter is related to the environmental profile of OPVs. OPVs have a much lower Cumulative Energy Demand, highlighting its manufacturing process is less energy intensive process, which leads to a lower Energy Payback Time as well. Moreover, since most of the contributions to

global warming come from electrical energy generation, OPVs could be marketed as being more sustainable

Author contributions

Manufacturer of BIM node and data acquisition – Noel Bristow, with support of Ferus Elliot. Analysis of measured climatic data and machine learning forecasting – Jeff Kettle with support of Tudur Wyn David. OPV and battery sizing work – Shoushou Zhang. Project concept Joe O'Mahony and Jeff Kettle. All authors contributed to the writing and proof reading.

Acknowledgements

Fergus Elliot gratefully acknowledge the financial support provided by the Knowledge Economy Skills Scholarships (KESS 2). JK would like to acknowledge the support of the University of Glasgow's EPSRC IAA grant (EP/R511705/1).

References

[1] Lee, H.K., Li, Z., Durrant, J.R. and Tsoi, W.C., 2016. Is organic photovoltaics promising for indoor applications?. *Applied Physics Letters*, *108*(25), p.253301.

[2] Ylikunnari, M., Välimäki, M., Väisänen, K.L., Kraft, T.M., Sliz, R., Corso, G., Po, R., Barbieri, R., Carbonera, C., Gorni, G. and Vilkman, M., 2020. Flexible OPV modules for highly efficient indoor applications. *Flexible and Printed Electronics*, *5*(1), p.014008.

[3] Hou, X., Wang, Y., Lee, H.K.H., Datt, R., Miano, N.U., Yan, D., Li, M., Zhu, F., Hou, B., Tsoi, W.C. and Li, Z., 2020. Indoor application of emerging photovoltaics—progress, challenges and perspectives. *Journal of Materials Chemistry A*, *8*(41), pp.21503-21525.

[4] Ma, L.K., Chen, Y., Chow, P.C., Zhang, G., Huang, J., Ma, C., Zhang, J., Yin, H., Cheung, A.M.H., Wong, K.S. and So, S.K., 2020. High-efficiency indoor organic photovoltaics with a band-aligned interlayer. *Joule*, *4*(7), pp.1486-1500.

[5] Kettle, J., Stoichkov, V., Kumar, D., Corazza, M., Gevorgyan, S.A. and Krebs, F.C., 2017. Using ISOS consensus test protocols for development of quantitative life test models in ageing of organic solar cells. *Solar Energy Materials and Solar Cells*, *167*, pp.53-59.

[6] A. S. Adila, A. Husam, and G. Husi, "Towards the self-powered Internet of Things (IoT) by energy harvesting: Trends and technologies for green IoT," *2018 2nd Int. Symp. Small-Scale Intell. Manuf. Syst. SIMS 2018*, vol. 2018-Janua, pp. 1–5, 2018.

[7] International Energy Agency, "Tracking Buildings 2020," 2020. [Online]. Available: https://www.iea.org/reports/tracking-buildings-2020.

[8] International Energy Agency, "Energy efficiency and digitalisation," 2019. [Online]. Available: https://www.iea.org/articles/energy-efficiency-and-digitalisation.

[9] L. Hernandez *et al.*, "A survey on electric power demand forecasting: Future trends in smart grids, microgrids and smart buildings," *IEEE Commun. Surv. Tutorials*, vol. 16, no. 3, pp. 1460–1495, 2014.

[10] S. Chalasani and J. M. Conrad, “A survey of energy harvesting sources for embedded systems,” *Conf. Proc. - IEEE SOUTHEASTCON*, pp. 442–447, 2008.

[11] B. H. Menze, B. M. Kelm, D. N. Splitthoff, U. Koethe, and F. A. Hamprecht, “On oblique random forests,” *Jt. Eur. Conf. Mach. Learn. Knowl. Discov. Databases*, pp. 453–469, 2011.

[12] D. L. Olson and D. Wu, “Regression Tree Models,” in *Predictive Data Mining Models*, Singapore: Springer, 2019, pp. 57–77.

[13] T. Hastie, R. Tibshirani, and J. Friedman, “Random forests,” in *The elements of statistical learning*, New York: Springer, 2009, pp. 587–604.

[14] L. Breiman, “Bagging predictors,” *Mach. Learn.*, vol. 24, no. 2, pp. 123–140, 1996.

[15] Google Maps, “School of Computer Science and Electronic Engineering [satellite image],” 2020. [Online]. Available: www.googlemaps.com. [Accessed: 12-Jun-2020].

[16] Bristow, N. and Kettle, J., 2018. Outdoor organic photovoltaic module characteristics: Benchmarking against other PV technologies for performance, calculation of Ross coefficient and outdoor stability monitoring. *Solar Energy Materials and Solar Cells*, *175*, pp.52-59.

[17] Kettle, J., Bristow, N., Sweet, T.K., Jenkins, N., dos Reis Benatto, G.A., Jørgensen, M. and Krebs, F.C., 2015. Three dimensional corrugated organic photovoltaics for building integration; improving the efficiency, oblique angle and diffuse performance of solar cells. *Energy & Environmental Science*, *8*(11), pp.3266-3273.

[18] Phillips, CoreLine Recessed LED lighting Product family leafet, 2021, April 8

[19] Weng, C.N., Yang, H.C., Tsai, C.Y., Chen, S.H., Chen, Y.S., Chen, C.H., Huang, K.M., Meng, H.F., Chao, Y.C., Chang, C.Y. and Zan, H.W., 2020. The influence of UV filter and Al/Ag moisture barrier layer on the outdoor stability of polymer solar cells. *Solar Energy*, *199*, pp.308-316.

[20] Soares, G.A., David, T.W., Anizelli, H., Miranda, B., Rodrigues, J., Lopes, P., Martins, J., Cunha, T., Vilaça, R., Kettle, J. and Bagnis, D., 2020. Outdoor performance of organic photovoltaics at two different locations: A comparison of degradation and the effect of condensation. *Journal of Renewable and Sustainable Energy*, *12*(6), p.063502.

[21] Salameh Ziyad M, Borowy Bogdan S. Methodology for optimally sizing of the combination of a battery bank and PV array in a wind/PV hybrid system. IEEE Transactions on Energy Conversion 1996;11(2):367–75.

[22] Shen, W. X. "Optimally sizing of solar array and battery in a standalone photovoltaic system in Malaysia." *Renewable energy* 34.1 (2009): 348-352.

[23] Lee, B., Lahann, L., Li, Y. and Forrest, S.R., 2020. Cost estimates of production scale semitransparent organic photovoltaic modules for building integrated photovoltaics. *Sustainable Energy & Fuels*, *4*(11), pp.5765-5772.

[24] Sopian, K., Cheow, S.L. and Zaidi, S.H., 2017, September. An overview of crystalline silicon solar cell technology: Past, present, and future. In *AIP Conference Proceedings* (Vol. 1877, No. 1, p. 020004). AIP Publishing LLC

[25] Gambhir, A., Sandwell, P. and Nelson, J., 2016. The future costs of OPV–A bottom-up model of material and manufacturing costs with uncertainty analysis. *Solar Energy Materials and Solar Cells*, *156*, pp.49-58.

[26] Aoki, Y., 2017. Photovoltaic performance of Organic Photovoltaics for indoor energy harvester. *Organic Electronics*, *48*, pp.194-197.

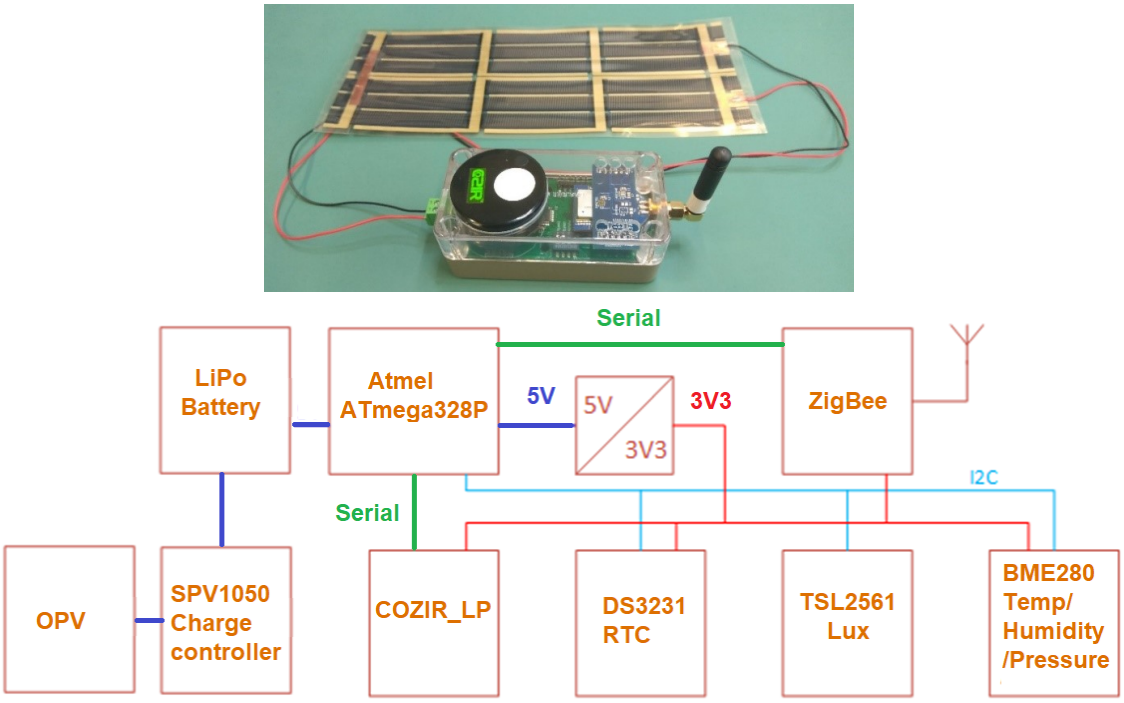

Figure 1(a) Photo of the Wireless sensor node (WSN) powered by flexible OPV module and (b) top-level schematic of the WSN system

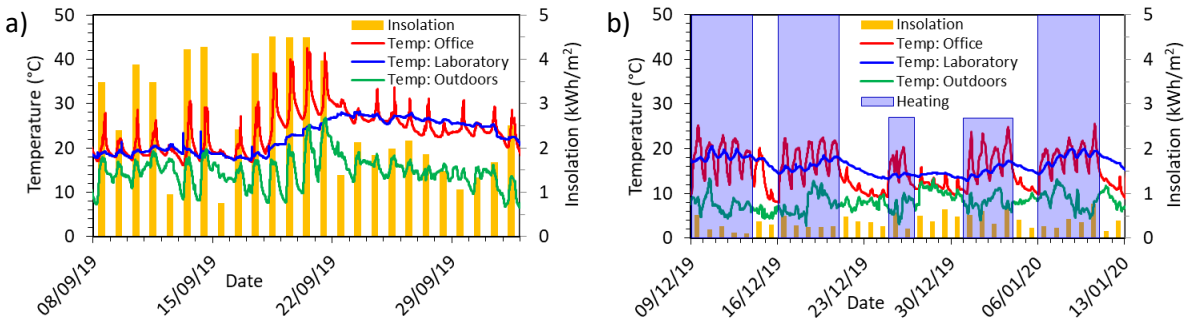

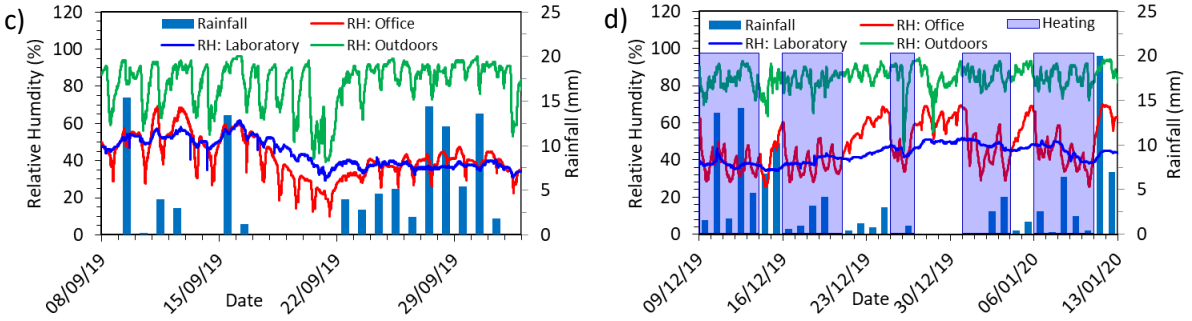

Figure 2: Temperature and relative humidity results: temperature and daily insolation for a) Summer 2019 and b) Winter 2019/20; relative humidity and rainfall for c) Summer 2019 and d) Winter 2019/20.

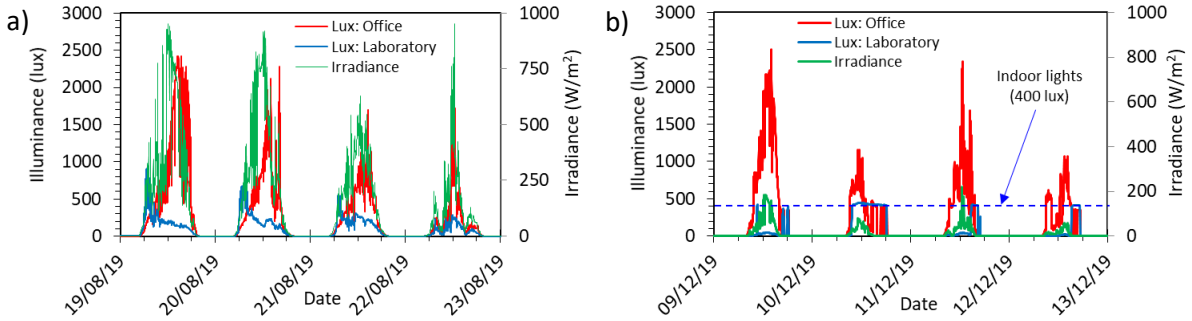

Figure 3: Indoor illuminance and outdoor irradiance: a) Summer 2019; and b) Winter 2019/20

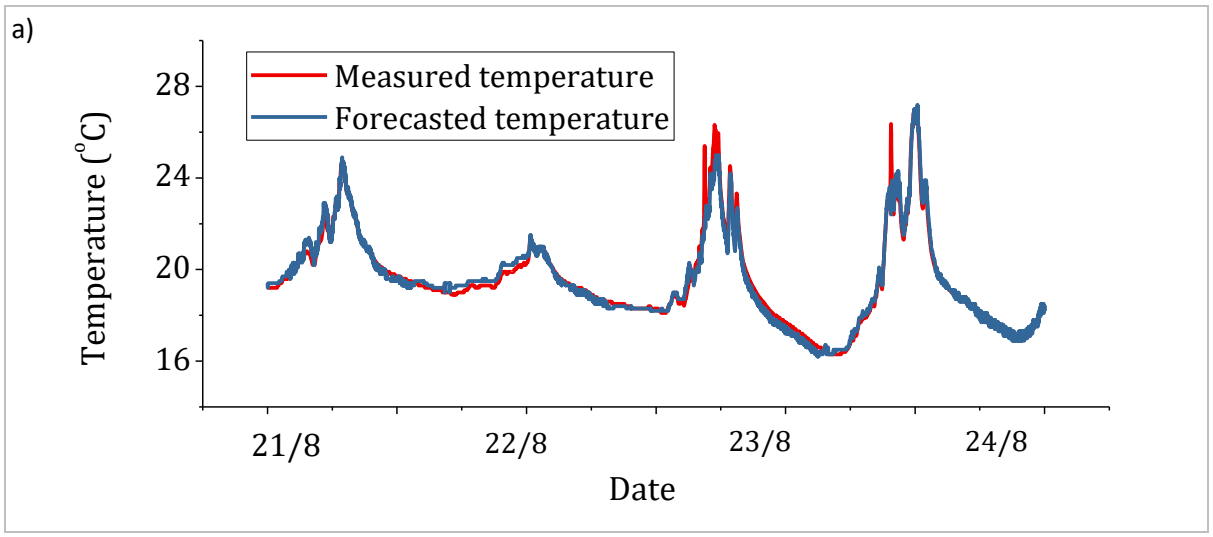

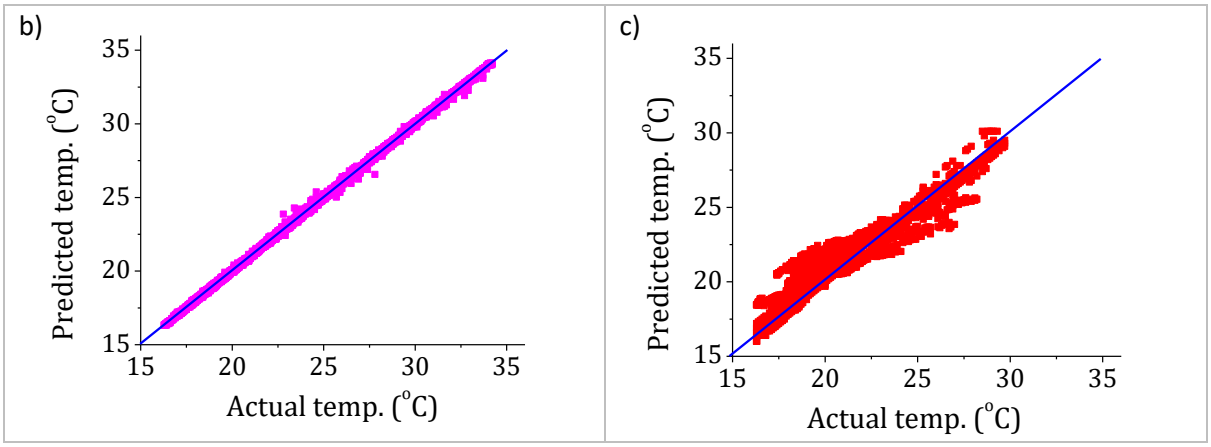

Figure 4: RF results for a testing set for Temperature in Office during Summer 2019: a) RF predicted and actual for both training and testing sets focusing on a cloudy and sunny day; b) RF predicted vs. actual for training set; c) RF predicted vs. actual for training set for testing set. In all data, 2 weeks of training and 2 weeks of testing data was used although only 4 days of data is shown in a)

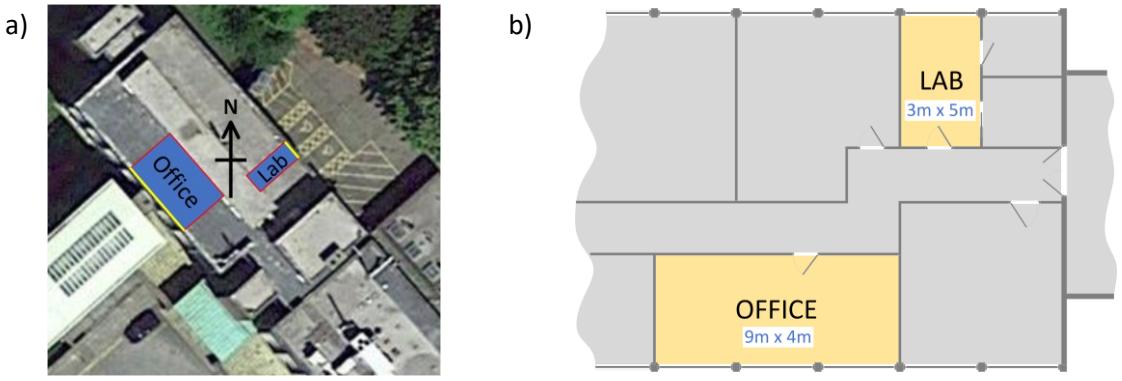

Figure 5: a) Aerial view of School of Electronics showing position and aspect of Lab and Office [16]. b) Floorplan of lab and office, showing comparative sizes of each room and highlighting the higher proportion of exterior walls/windows in the office compared to the lab.

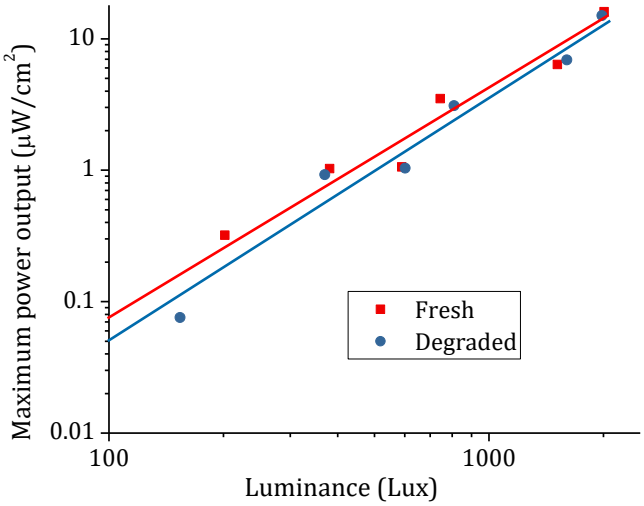

Figure 6: Performance of the OPV used in this work, showing how the maximum output power varies as a function of luminance (Lux). The initial measurements were taken in June 2019. When modules were tested after 22 months later (April 2021), a small decrease in OPV output power was noted at low luminance (at 200 Lux, -26% relative drop in performance) and only a minor drop was noted at high luminance (at 1000 Lux, -11% relative drop in performance).

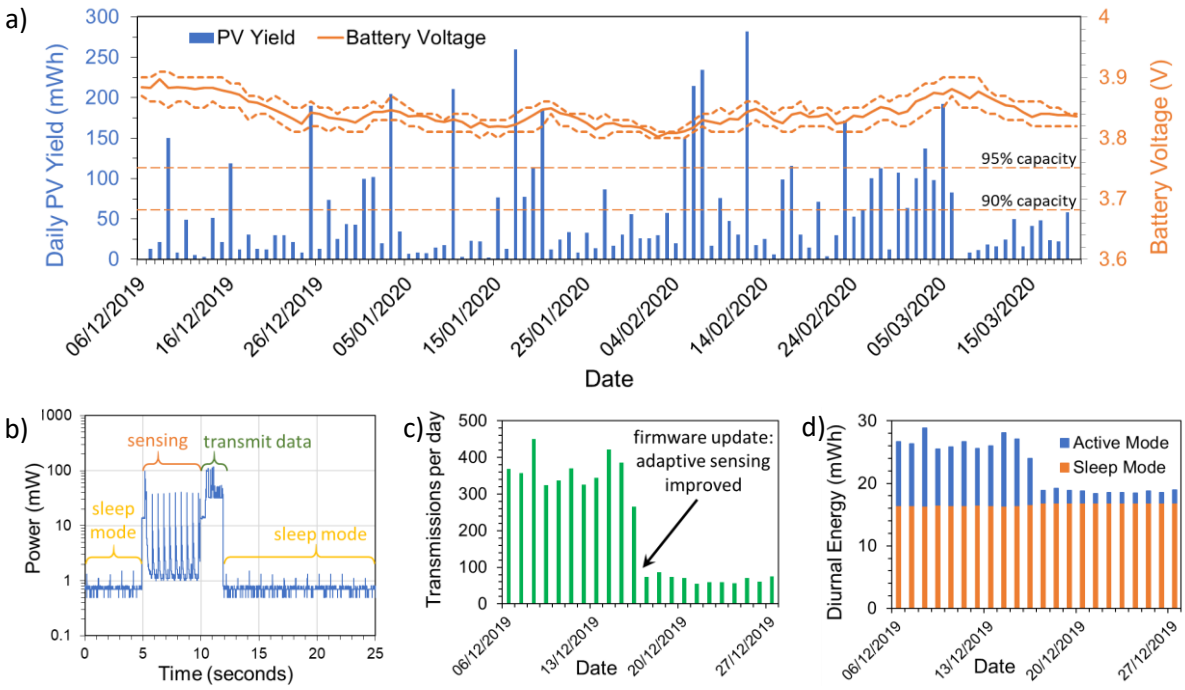

Figure 7: a) Figure 10: Diurnal energy yield from OPV module and sensor node battery voltage (average, maximum and minimum). Battery storage capacities at 90% (3.68V) and 95% (3.75V) are shown. b) Detail of power usage by the node during sleep and sensing/transmission cycle. c) No of wireless sensor node transmissions per day. d) Diurnal energy used by the node in active and sleep modes.

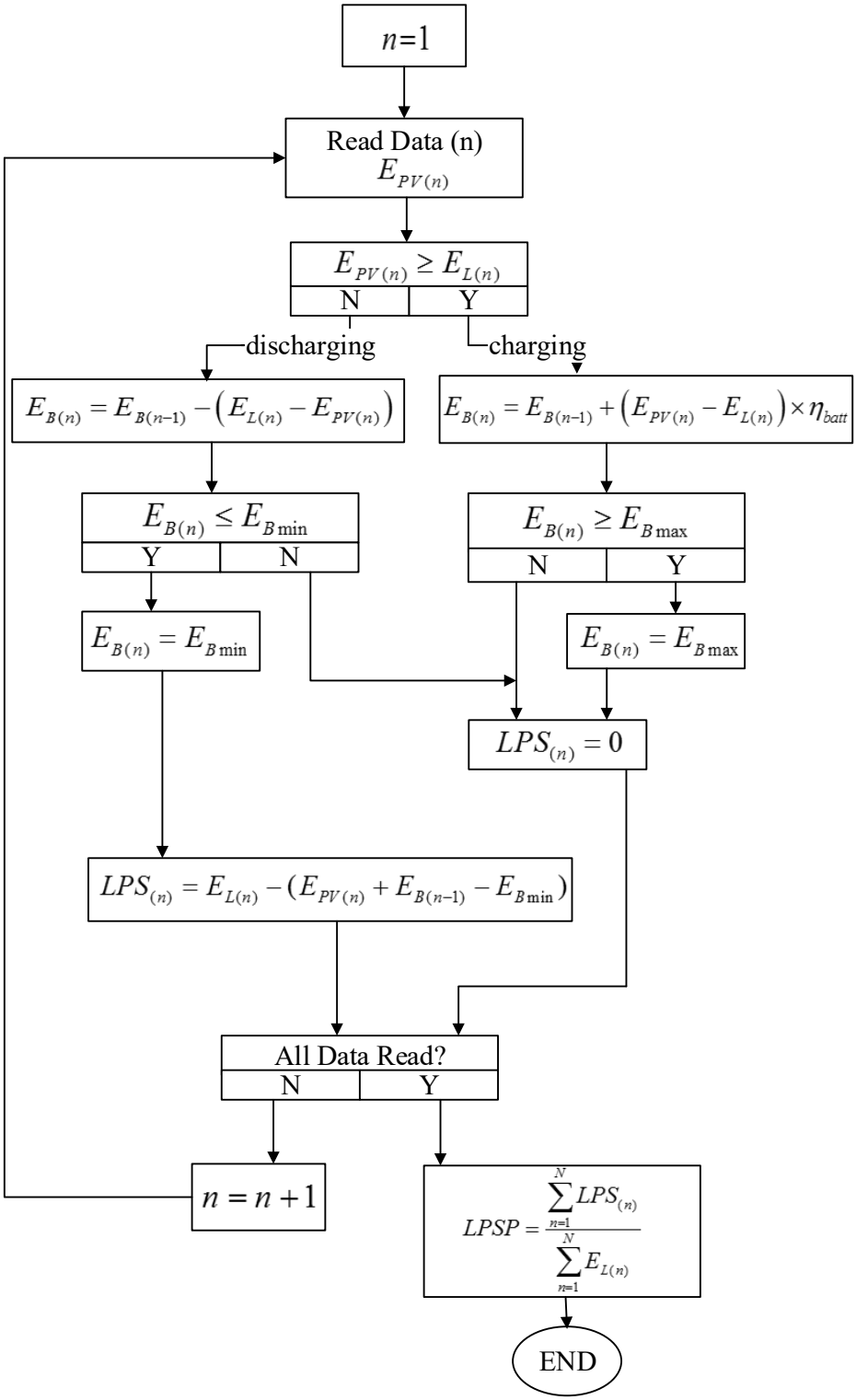

Figure 8; Flowchart graph used for the calculation of LPSP for varying OPV sizes, battery sizes and load demands

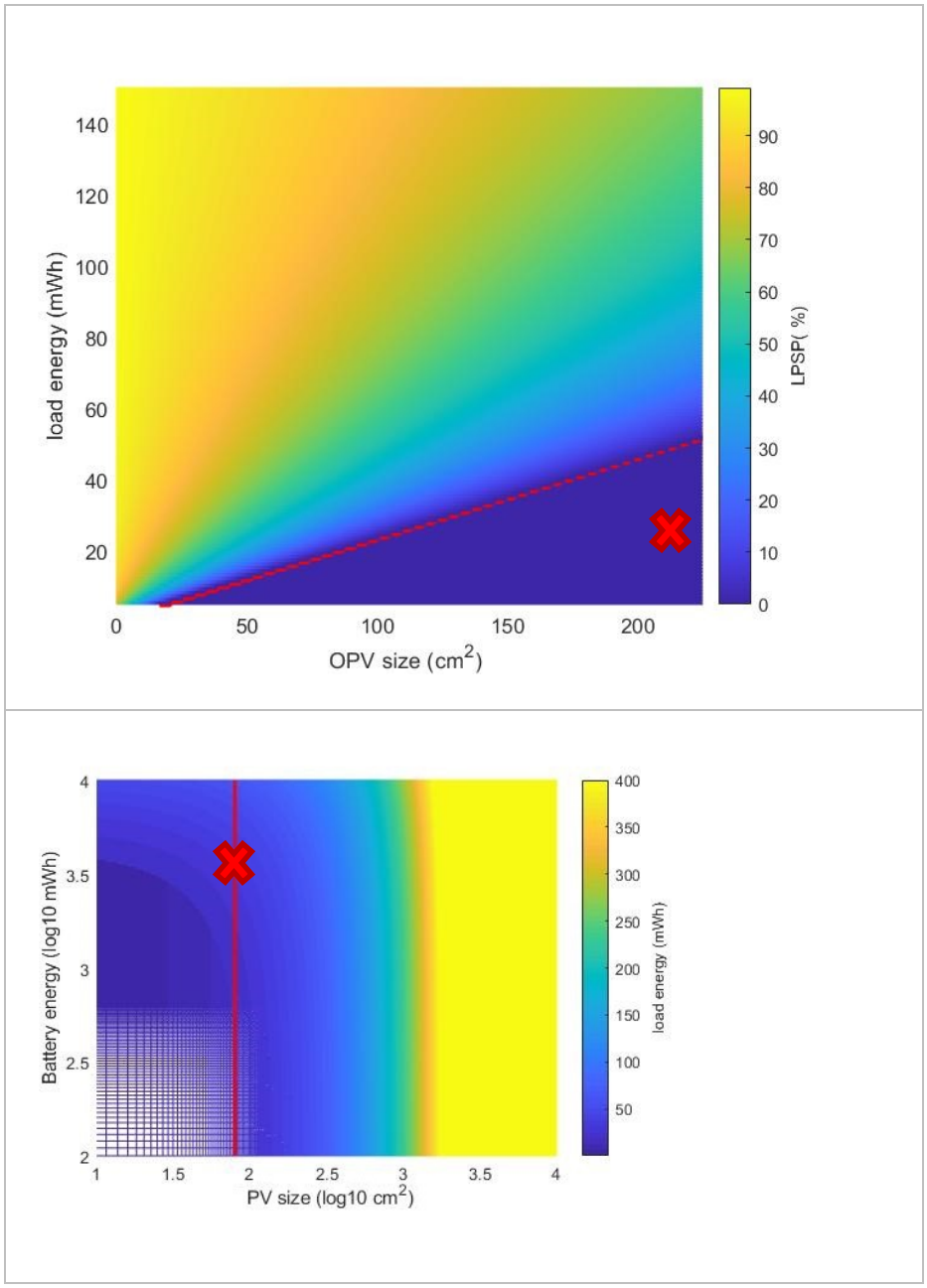

Figure 9 (a) Effect of OPV module size and load demand (at a fixed battery size 3700mWh) effect the 'loss of load probability' (LPSP). Data points below the red line indicate that an LPSP = 0.01 is obtained. Figure (b) shows the minimum load demand that can be met for a particular combination of PV size and battery size for the desired LPSP=0.01. The white section indicates it is not possible to power the WSN in this range.